GMR
The Original

SOLUTION COMBUSTION SYNTHESIS OF $MGAL_2O_4$ AT 800^OC SPINEL NANOPARTICLES: STRUCTURAL CHARACTERISATION AND PHOTOCATALYTIC DEGRADATION OF CORALENE DARK RED 2B

Rakshit Hosamani[1], Yogendra. K[2], Kartheek B S[3], Sujeetkumar M Dongre[4], Rakesh Tiwari[5], Madhusudhana Narayanappa[6], Shiva. Naik.H[7]

[1]Department of PG Studies and Research in Environmental Science, Kuvempu University, India: Shimoga, Karnataka, India. Email: rakshithosamani27@gmail.com, 0009-0000-8448-6383
[2]Department of PG Studies and Research in Environmental Science, Kuvempu University, India: Shimoga, Karnataka, India. Email: yogendraku@gmail.com 0000-0001-8652-8444
[3]Civil Engineering Department College Bangalore Institute of Technology, Email: karthikbs@bit-bangalore.edu.in
[4]Department of PG Studies and Research in Environmental Science, Kuvempu University, India: Shimoga, Karnataka, India. Email: dongresujeet@gmail.com, 0009-0005-6994-8566
[5]Department of PG Studies and Research in Environmental Science, Kuvempu University, India: Shimoga, Karnataka, India. Email: shimogarakesh@gmail.com Orcid id: https://orcid.org/0000-0002-2191-769X
[6]Department of PG Studies and Research in Environmental Science, Kuvempu University, India: Shimoga, Karnataka, India. Email: madhubdvt@gmail.com Orcid id: 0000-0002-8804-6294
[7]Department of PG Studies and Research in Environmental Science, Kuvempu University, India: Shimoga, Karnataka, India. Email: shivanaikh1234@gmail.com; Orcid id: 0009-0000-2191-9639

ABSTRACT

$MgAl_2O_4$ nanoparticles were prepared by solution combustion of magnesium and aluminium nitrates with urea as fuel, followed by calcination at 800 °C. XRD showed phase-pure cubic spinel (JCPDS 21-1152, Fd-3m) with no MgO or Al_2O_3 impurities. UV–Vis spectroscopy showed strong absorption below 250 nm and almost none in the visible range. TEM showed rounded, partly fused grains of about 100–300 nm, and SAED confirmed their crystallinity. SEM showed angular, micrometre-sized aggregates, and EDX detected only O, Mg and Al. Photocatalytic activity was tested on 200 ppm Coralene Dark Red 2B under LED light (1200 µmol m^{-2} s^{-1} PAR, pH 7, 180 min) at ten catalyst loadings (1.6–130 g L^{-1}), with dark controls run in parallel. Dye removal stayed above 96.5% at every loading, reaching 99.8% in the light and 99% in the dark. Light and dark results were close, so adsorption on the powder accounted for most of the removal.

KEYWORDS: $MgAl_2O_4$; spinel; solution combustion; photocatalysis; Coralene Dark Red 2B

INTRODUCTION

Water pollution caused by synthetic dyes has become one of the more stubborn environmental problems of modern industry. Dyes are used in textiles, leather, paper, plastics, printing, cosmetics and food, and world production is put at more than 700,000 tons a year [1]. A noticeable share of the dye that is used never binds to the fiber and ends up in the wastewater. Most dyes are built to resist light, heat and washing, which is why they persist in water bodies once released. Coloured effluent blocks sunlight, which lowers photosynthesis and dissolved oxygen, and many dyes, especially azo dyes, can break down into aromatic amines that are toxic and in some cases carcinogenic or mutagenic [2].

Textile dyes are usually grouped by chemical structure or by the way they are applied to the fiber, and the main application classes are reactive, direct, disperse, vat, sulphur, acid and basic dyes [3]. Most commercial colourants, in particular the azo dyes, carry one or more –N=N– groups attached to aromatic rings, a structure that resists ordinary biological breakdown. Reactive dyes are lost in especially large amounts, since part of the dye reacts with water in the bath instead of the fiber. Textile wastewater is a mixture of dyes and many other contaminants, which makes it harder to treat, and legislation commonly requires factories to treat it before it is discharged into the receiving watercourses [4].

Conventional treatment methods such as coagulation, adsorption, membrane filtration and biological treatment each have limits. Several of them only move the dye from the water into a solid phase, leaving sludge that needs further disposal, and many dyes are too complex for microorganisms to break down. Heterogeneous photocatalysis offers a different route. When a semiconductor absorbs light of sufficient energy it creates electron–hole pairs, which produce reactive species such as hydroxyl and superoxide radicals. These attack the dye molecule and can mineralize it into carbon dioxide, water and simple inorganic ions [5]. The idea goes back to early work on light-driven reactions at semiconductor electrodes [6], and the search for catalysts that are cheap, stable, non-toxic and easy to make remains an active area of research.

Researchers at Kuvempu University have followed this approach for several years, using nanoparticles synthesized in the laboratory to remove textile dyes from water. Madhusudhana et al. [7] reported the photocatalytic decolorization of textile effluent using synthesized nanoparticles, and Santhosh *et al.* [8] prepared nickel calcite nanoparticles by solution combustion and examined their photodegradation efficiency. Metal oxides made by simple routes of this kind are attractive because they work under ultraviolet or solar light, need no special reagents, and can be scaled up from a laboratory preparation.

Magnesium aluminate ($MgAl_2O_4$) is one material that fits this description. It crystallises in the cubic spinel structure (space group Fd-3m), in which magnesium and aluminium occupy tetrahedral and octahedral sites of a close-packed oxygen lattice, although a degree of cation exchange between the two sites is common in real samples [9]. The spinel is known for its high melting point, chemical inertness, good mechanical strength and wide band gap, and it is made from two abundant, inexpensive elements [10].

Its use as a photocatalyst for dyes has been reported by several groups, including the removal of malachite green under solar light [11], direct green 6 [12] and Coralene Blue BGFS under UV light [13]. Taken together, these studies show that the spinel and its related aluminates can decolourise dyes of different types, which makes the material worth studying in more detail.

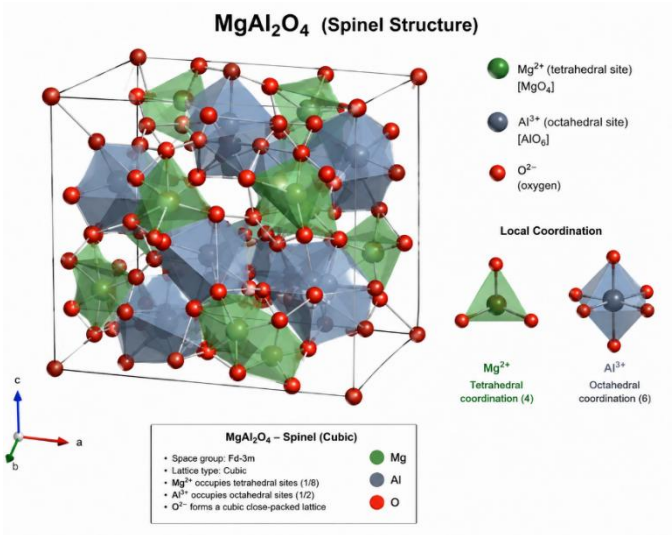
The ideal crystal has a very wide band gap, so it absorbs mainly in the deep ultraviolet and is transparent in the visible region. In practice, however, defects, oxygen vacancies and surface states created during synthesis introduce extra energy levels inside the gap, and these are thought to be responsible for the absorption features and photocatalytic response seen in real powders [14]. Particle size, surface area and defect content therefore matter as much as the crystal structure itself, and all three are controlled by the way the powder is made. Nanoparticles prepared by sol–gel auto-combustion have also shown photocatalytic properties [15].

The properties of $MgAl_2O_4$ depend strongly on how it is prepared. Conventional solid-state reaction needs very high temperatures and long heating times and tends to give coarse particles. Wet-chemical routes such as co-precipitation give finer powders [16], but they need several steps and careful control of the precipitating conditions. Solution combustion synthesis is a simpler alternative. Metal nitrates act as oxidizers and an organic fuel, commonly urea, drives a rapid, self-sustaining exothermic reaction [17], so that a fine powder forms in minutes with little external energy, and the large volume of gas released helps to keep the particles from growing together too much [18].

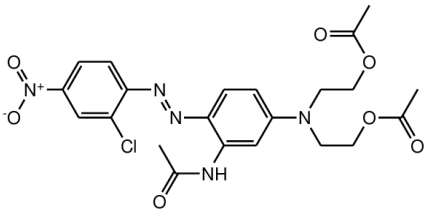
The method has been reviewed in detail for nanoscale materials in general [19] and has been applied to $MgAl_2O_4$ through auto-ignition [20] and microwave-assisted combustion [21], where nanocrystalline spinel powders were obtained. Because the product depends on the fuel, the oxidizer-to-fuel ratio and the heating conditions, these variables have to be chosen with care.

The amount of urea used is known to affect the properties of the spinel obtained [22]. Combustion products are also often only partly crystalline and may contain residual carbon or nitrogen compounds, so a calcination step is used to complete crystallization. A higher temperature gives better crystallinity but also promotes sintering, in which neighboring grains fuse and the surface area falls [23]; in this work 800 °C was chosen because it is high enough to form the spinel phase and low enough to limit sintering. Mixed-oxide nano-catalysts from the same research group have also been used as recyclable catalysts in organic synthesis [24].

In this work, $MgAl_2O_4$ nanoparticles were prepared by solution combustion of magnesium and aluminium nitrates with urea as the fuel, followed by calcination at 800 °C. The product was characterised by X-ray diffraction for the crystalline phase [25], UV–Vis absorption spectroscopy for the optical behaviour, transmission electron microscopy with selected area electron diffraction for particle shape and crystallinity [26], and scanning electron microscopy with energy-dispersive X-ray spectroscopy for surface morphology and elemental composition [27]. The photocatalytic activity of the powder was then tested on Coralene Dark Red 2B, an azo textile dye, under LED illumination. The aims were to obtain phase-pure, crystalline $MgAl_2O_4$ by a simple combustion route, to describe its structure, morphology and composition, and to examine how the catalyst loading affects dye degradation.



3D Structure of MgAl2O4



Structure of Coralene Dark Red 2B Dye

2. MATERIALS AND METHODS

2.1. Chemicals and materials

The chemicals used for the synthesis of $MgAl_2O_4$ nanoparticles were magnesium nitrate ($Mg(NO_3)_2 \cdot 6H_2O$, 98%), aluminium nitrate ($Al(NO_3)_3 \cdot 9H_2O$, 98%) and urea (CH_4N_2O, [100.50%]) as the fuel, purchased from LOBA Chemie Pvt. Ltd., Mumbai, Maharashtra, India. Metal nitrates of this kind are the standard oxidiser precursors for solution-combustion synthesis of magnesium aluminate [12]. All chemicals were of analytical grade and were used without further purification. Double-distilled water was used as the solvent throughout the experiment. Coralene Dark Red 2B, an azo textile dye, was used as the model pollutant in the photocatalytic experiments.

2.2. Synthesis of $MgAl_2O_4$ nanoparticles

$MgAl_2O_4$ nanoparticles were synthesised by a simple solution combustion method [17, 19], in which the metal nitrates act as oxidisers and urea acts as the fuel in a self-propagating reaction [24]. The oxidiser-to-fuel ratio was calculated from propellant chemistry [28], with a Mg:Al molar ratio of 1:2.

Magnesium nitrate (7.69 g) and aluminium nitrate (22.50 g) were dissolved in 20 mL of double-distilled water, and urea (12.10 g) was added under constant stirring. The clear solution was placed in a preheated muffle furnace at 800 °C [13]. The solution boiled and dehydrated, then ignited [20]. A large volume of gas evolved and a voluminous, foamy powder remained [18]. The as-burnt powder was ground thoroughly [8] and calcined in air at 800 °C for [4 hours] at a heating rate of 8000C to obtain the final $MgAl_2O_4$ nanoparticles.

2.3. Characterisation of the nanoparticles

The crystalline phase was identified by powder X-ray diffraction (XRD) on a Rigaku Ultima-IV X-ray diffractometer using Cu-Kα radiation (λ = 1.5406 Å) over a 2θ range of 5°–90° [25]. The peaks were indexed against JCPDS card No. 21-1152 [29]. Optical absorption was recorded on a Spectro-2080 double-beam spectrometer over 200–800 nm [30]. Particle morphology was examined by transmission electron microscopy (TEM; JEOL JEM-2100Plus), and selected area electron diffraction (SAED) was used to confirm crystallinity [31]. For TEM, the powder was dispersed in ethanol by ultrasonication and drop-cast on a carbon-coated copper grid. Surface morphology was studied by scanning electron microscopy (SEM; model JSM-IT500 LA In Touch Scope) at magnifications from 200X to 25.00KX [32]. Elemental composition was determined by energy-dispersive X-ray spectroscopy (EDX) attached to the SEM, from the region marked “Spectrum 1” [33].

2.4. Photocatalytic experiment

Photocatalytic degradation of Coralene Dark Red 2B dye was carried out under artificial illumination provided by a Hainu LED floodlight (model HN-AF2436C; input 110–265 V, output 900 mA ± 5%, 26–36 V, maximum 42 V), placed 10 cm above the reaction chamber. The photon flux density inside the chamber was measured with a MultispeQ (PAR) instrument (PhotosynQ Inc., East Lansing, MI, USA) and maintained at 1200 µmol m^{-2} s^{-1} (PAR) throughout all experiments [34].

A 200 ppm stock solution of Coralene Dark Red 2B was prepared by dissolving the dye in double-distilled water to a final volume of 1000 mL. For each experiment, 10.0 mL of the stock solution was taken in a borosilicate glass beaker, and the synthesised $MgAl_2O_4$ nanoparticle catalyst was added at one of ten loadings (0.016, 0.032, 0.065, 0.130, 0.260, 0.325, 0.520, 0.780, 1.040 and 1.300 g, equivalent to 1.6–130.0 g L^{-1}) under continuous magnetic stirring. The suspension pH was adjusted to and maintained at neutral (pH ≈ 7) using 0.01 N NaOH or 0.01 N HCl as required, and the mixture was then exposed in the light chamber for 180 min. Dark-control experiments were carried out in parallel for every catalyst loading, using the same 200 ppm dye concentration under identical conditions but with the chamber protected from light. Over the course of the reaction, the suspended catalyst settled to the bottom of the beaker under gravity, leaving a clear supernatant above the sediment. A 200 µL portion of this clear supernatant was transferred to designated wells of a 96-well microplate. Full absorbance spectra (200–1000 nm, 1 nm interval) were recorded on a Multiskan Sky microplate spectrophotometer (Thermo Fisher Scientific, Waltham, MA, USA; serial no. 1530-800239C; firmware v1.0.55; software v1.44.16.0), with the cuvette port enabled and the plate chamber held at 25 °C. All experiments were performed in quintuplicate (n = 5) for each catalyst dosage, under both irradiated and dark conditions, and results are reported as mean ± standard deviation, with one-way ANOVA performed. Data processing and statistical analysis were performed in R (v4.5.1); dose–response relationships between catalyst loading and degradation efficiency were modelled using a power function for light and a linear fit for dark conditions, and all plots were generated with the ggplot2 package.

3. RESULTS AND DISCUSSION

3.1. X-ray diffraction (XRD)

Figure 1 shows the XRD pattern of the sample calcined at 800 °C, scanned from 5° to 90° (2θ). Six clear peaks appear at 18.96°, 31.60°, 37.03°, 44.86°, 59.73° and 65.32°. These are indexed to the (111), (220), (311), (400), (511) and (440) planes of cubic $MgAl_2O_4$ spinel and line up closely with the standard reference pattern JCPDS Card No. 21-1152 (space group Fd-3m, a = 8.083 Å) [16, 29]. The peaks are sharp and there are no extra peaks from leftover MgO or Al_2O_3, so the sample is a clean, well-crystallised single phase of $MgAl_2O_4$ [22].

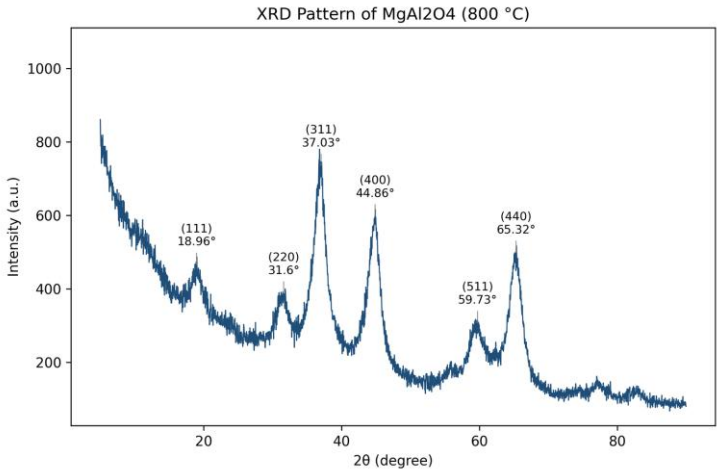


Figure 1. XRD pattern of $MgAl_2O_4$ calcined at 800 °C, with peaks indexed to their (hkl) planes.

Table 1. XRD peak positions of $MgAl_2O_4$ indexed against JCPDS 21-1152.

2θ (°)	(hkl)	Relative intensity (%)*
18.96	111	35
31.60	220	–
37.03	311	100
44.86	400	65
59.73	511	–
65.32	440	55

*Relative intensity is scaled to the strongest (311) peak, as reported for JCPDS 21-1152.

3.2. UV–Vis absorption spectroscopy

Figure 2 shows the UV–Vis absorption spectrum of the sample, scanned from 200 to 800 nm. Absorbance rises sharply below 250 nm, and two smaller peaks appear around 273 nm and 372 nm. These are likely due to charge-transfer transitions and defect or surface states in the $MgAl_2O_4$ lattice [14]. This is expected for $MgAl_2O_4$, which is a wide-band-gap oxide and appears optically transparent in the visible range [11].

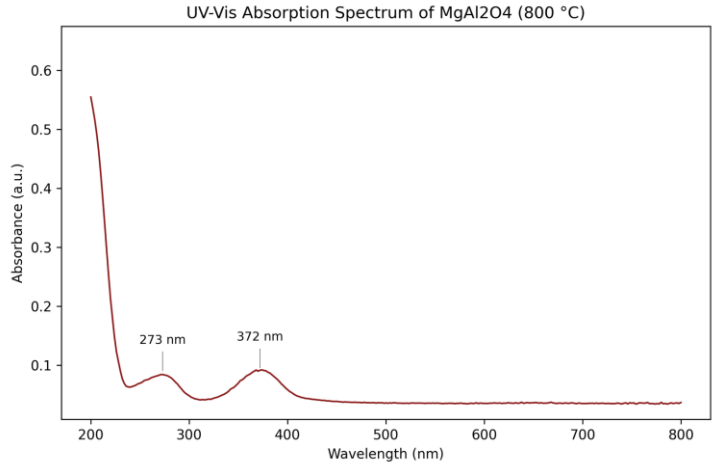


Figure 2. UV–Vis absorption spectrum of $MgAl_2O_4$ calcined at 800 °C.

3.3. Transmission electron microscopy (TEM)

3.3.1. Morphology

The TEM images (Figure 3) show that the particles are mostly rounded to slightly polyhedral in shape, and they tend to stick together in clusters rather than sitting apart as separate grains. At lower magnification (Figure 3b) a fairly large, dense agglomerate made up of many smaller grains packed tightly together is visible [21]. The particles range from about 100 to 300 nm and appear smooth and rounded, with their edges fused together. Because the particles are so closely packed and overlapping, it is hard to pick out clean, separate boundaries for every particle, which is common for oxide powders made by high-temperature calcination, since the heat tends to fuse neighboring grains together (a process called sintering or necking) [23].

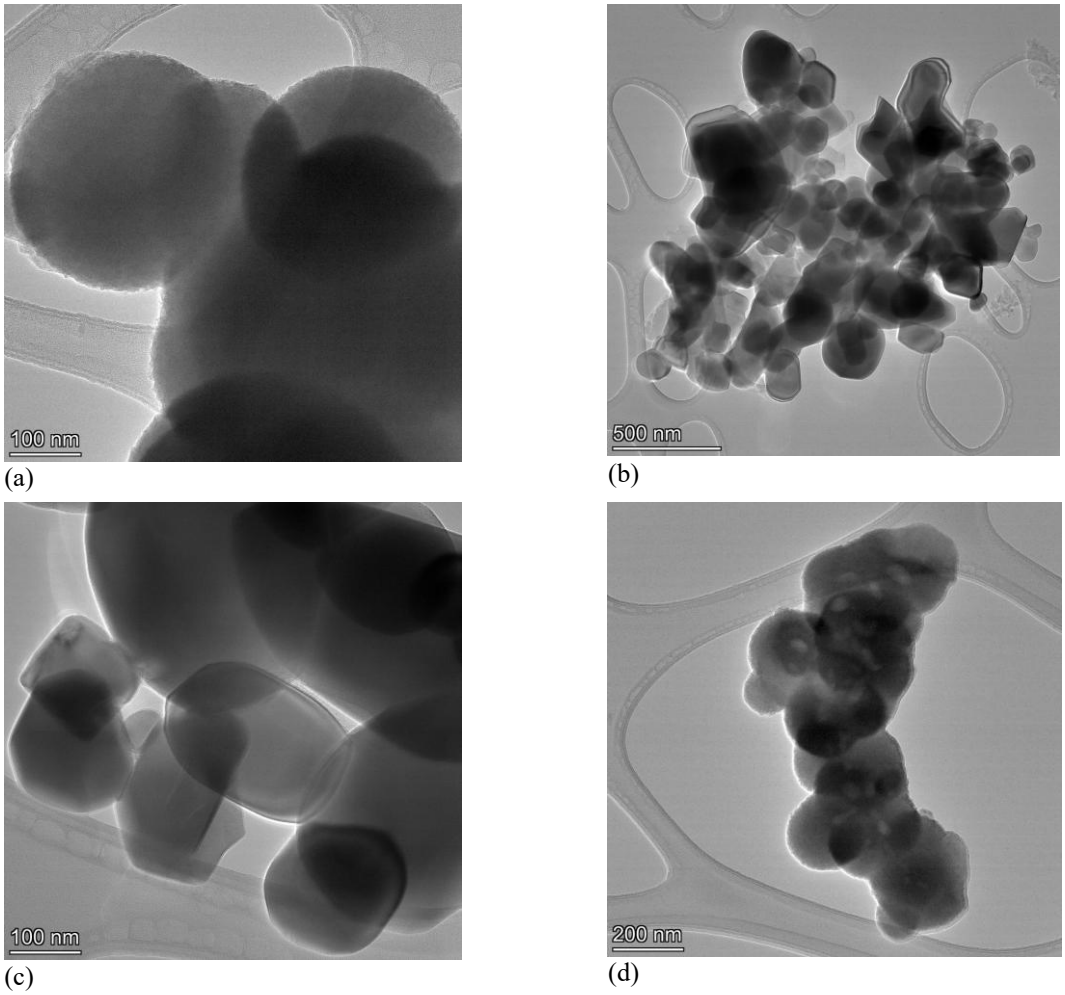


Figure 3. TEM images of $MgAl_2O_4$: (a) individual rounded grains (scale bar: 100 nm); (b) lower-magnification view of a larger agglomerate of particles (scale bar: 500 nm); (c) close-up view of fused (necked) grains (scale bar: 100 nm); (d) chain-like cluster of particles (scale bar: 200 nm).

3.3.2. Selected area electron diffraction (SAED)

Figure 4 shows the SAED pattern taken from the particles. Instead of a plain diffuse halo (which would mean the material is amorphous), the pattern shows a series of bright spots arranged in a ring-like fashion. This is a clear sign that the particles are crystalline, not glassy or amorphous, and it agrees with the sharp, well-defined peaks already seen in the XRD pattern of the $MgAl_2O_4$ spinel phase [26].

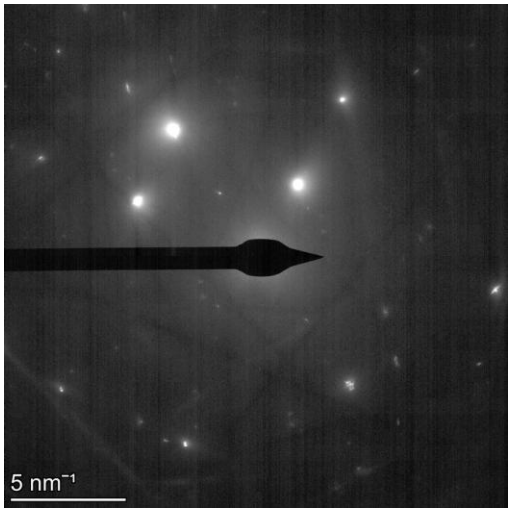


Figure 4. SAED pattern of $MgAl_2O_4$ confirming its crystalline nature.

3.4. Scanning electron microscopy (SEM)

SEM displays the surface morphology of the powder over a significantly larger field of view than TEM, which is beneficial for seeing how the particles appear in bulk rather than individually [35]. Figure 5 shows the sample at increasing magnification, from 200X to 25.00KX. At low magnification (Figure 5a), the powder looks like a rough, uneven surface scattered with small angular fragments of different sizes; there is no obvious repeating pattern, just a jumbled mix of grains sitting on top of a coarser base layer. At higher magnification (Figures 5b–5d), the picture becomes much clearer: the material is made up of irregular, sharp-edged, plate- and block-like chunks that look as if they have been fractured or crushed, which is typical for a ceramic powder that has been calcined and then ground [15]. At the highest magnification (Figure 5d), the surfaces of these bigger chunks are not smooth at all. They are dotted with many tiny, rounded particles and fine debris, giving the surface a rough, grainy texture rather than a flat, glassy one.

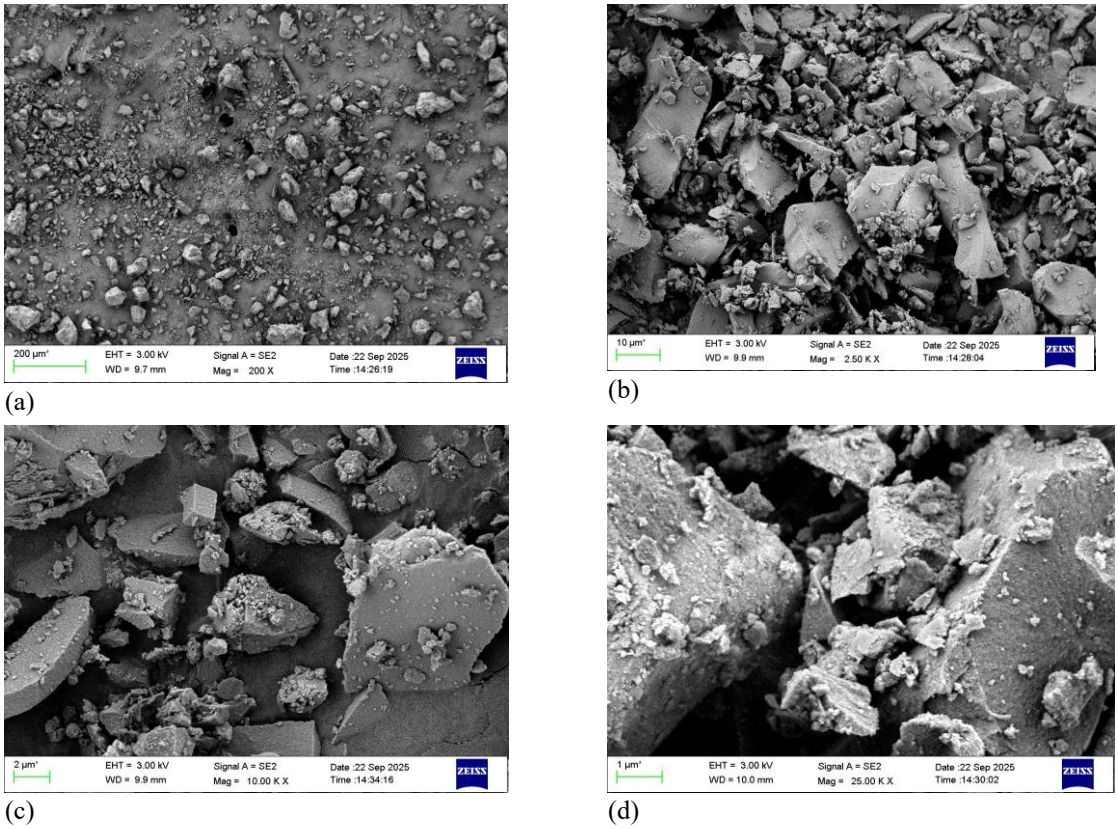


Figure 5. SEM images of $MgAl_2O_4$ at increasing magnification: (a) overall powder surface (200X, scale bar: 200 µm); (b) irregular, fractured particle chunks (2.50KX, scale bar: 10 µm); (c) angular, plate-like grains with fine particles on their surface (10.00KX, scale bar: 2 µm); (d) rough, grainy surface texture of a single chunk (25.00KX, scale bar: 1 µm).

3.5. Energy-dispersive X-ray spectroscopy (EDX)

Figure 6 shows the scanned area (labelled Spectrum 1), and Figure 7 shows the resulting spectrum. Only three peaks appear in the spectrum, oxygen, magnesium and aluminium, and there is nothing else, indicating that no other elements were picked up in detectable amounts during this scan [27].

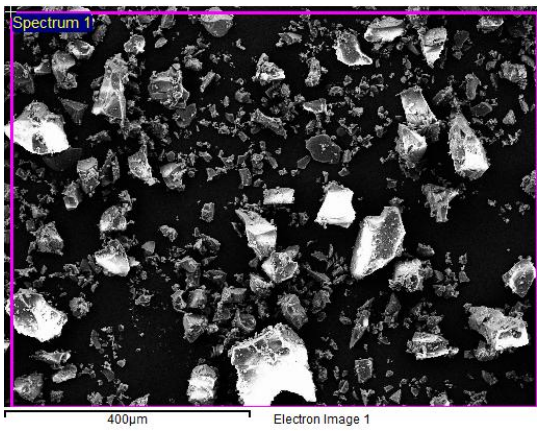


Figure 6. SEM image of the scanned region, with the EDX spectrum collection area marked "Spectrum 1" (scale bar: 400 µm).

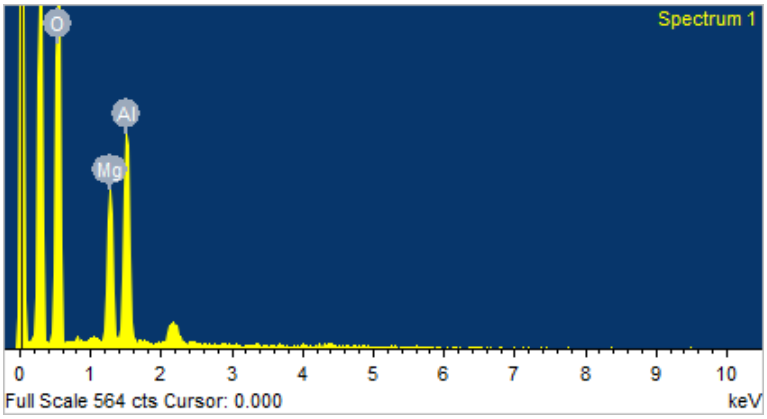


Figure 7. EDX spectrum of the sample, showing peaks for O, Mg and Al only.

Table 2 gives the weight and atomic percentages calculated from the spectrum, and Figure 8 compares them. Oxygen accounts for the majority of the signal, which makes sense given that it is the lightest and most plentiful element in an oxide, followed by aluminium and magnesium. The three elements add up to 100%, indicating that the analysis was limited to O, Mg and Al (no carbon, gold coating or other stray elements were counted).

Table 2. EDX quantitative results for the $MgAl_2O_4$ sample.

Element	Weight (%)	Atomic (%)
O	60.51	71.25
Al	24.06	16.79
Mg	15.43	11.96
Total	100.00	100.00

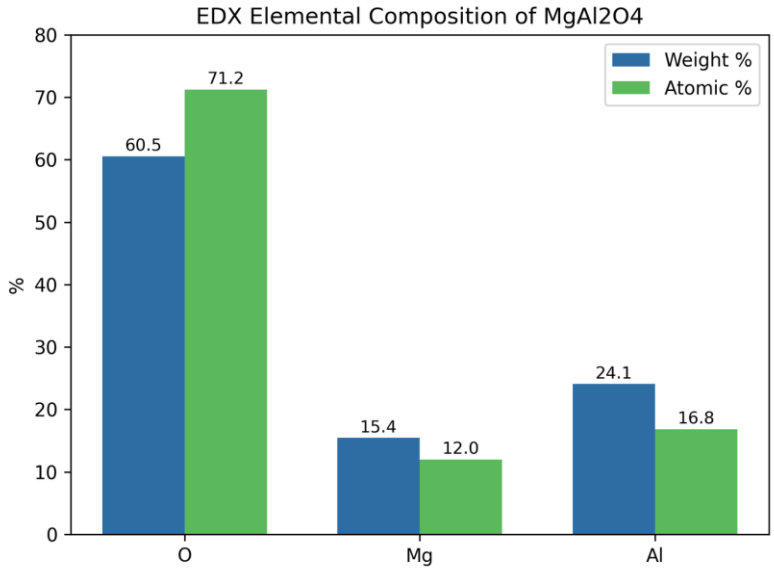


Figure 8. Bar chart comparing weight % and atomic % of O, Mg and Al.

3.6. Photocatalytic degradation of Coralene Dark Red 2B

Figure 9 shows how 200 ppm Coralene Dark Red 2B was removed over 180 min at pH 7, in the light and in the dark, at the catalyst loadings tested (0.016–1.300 g in 10 mL). On the x-axis the loadings are labelled as catalyst dosage (ppmv). Removal was worked out from the absorbance of the clear supernatant at the main absorption peak of the dye, and the specific removal capacity (qg, g of dye removed per g of catalyst) was calculated from the same readings.

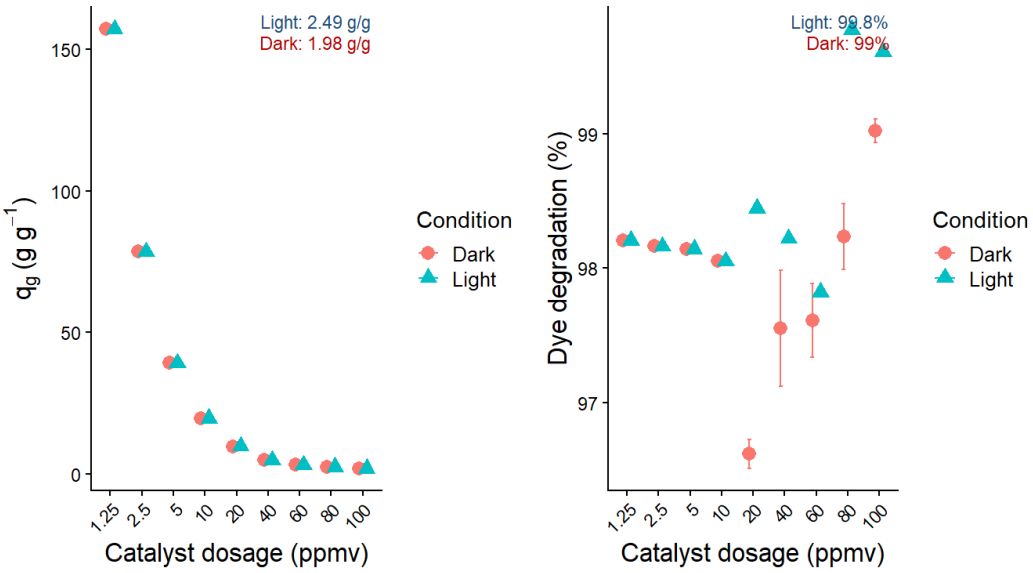


Figure 9. Effect of $MgAl_2O_4$ dosage on Coralene Dark Red 2B removal after 180 min (200 ppm dye, pH 7). Left: specific removal capacity (qg, g g^{-1}). Right: dye degradation (%). Triangles show LED light and circles show the dark control; points are means and error bars show the standard deviation (n = 5).

Catalyst dosage had a strong effect on qg but only a small effect on the overall removal of dye. qg dropped from about 157 g g^{-1} at 1.25 ppmv to 2.49 g g^{-1} in the light and 1.98 g g^{-1} in the dark at the highest dosage, roughly halving each time the dosage doubled. This is what one would expect when the dye load is fixed, because extra catalyst adds mass without taking out much more dye [36, 37]. Removal stayed above 96.5% in every treatment. Between 1.25 and 10 ppmv the light and dark results were almost the same (about 98.1–98.2%), which suggests that adsorption dominated. At higher dosages the two conditions began to separate. Removal in the light was higher at 20 ppmv (about 98.5% against 96.6% in the dark) and at 80 ppmv, and the maximum was 99.8% in the light against 99% in the dark. [Add the fitted equations with R^2 for light (power) and dark (linear), and the ANOVA F and p values.]

The light advantage is small, about 2 percentage points at most, and it shows up only at some of the higher dosages. Most of the colour removal in these runs is therefore best put down to adsorption on the powder, with photogenerated charge carriers adding a little on top [5, 38]. A small light effect is not surprising for this material. The UV–Vis spectrum (Section 3.2) shows almost no absorption in the visible range, and the LED source emits mainly visible light, so excitation across the band gap should be limited and any response probably comes through the defect or surface states mentioned earlier [14]. Visible-light activity has been reported for $MgAl_2O_4$ made by urea-fuelled combustion [34], although later work attributed it to nitrogen doping rather than to the spinel itself [14]. Earlier studies on $MgAl_2O_4$ and related aluminates used UV or solar light, and in one case added H_2O_2 [11, 13]. Here no oxidant was added, which may also help to explain the modest light effect.

The dip at 20 ppmv in the dark and the large error bars at intermediate dosages may reflect particle aggregation and light scattering [39]. This fits the TEM and SEM images, which show that the powder exists mostly as large agglomerates and not as separate grains, so a good part of the surface is not exposed to the dye.

3.7. Overall discussion

Taken together, the characterisation techniques and the photocatalytic tests build a consistent picture of the sample calcined at 800 °C.

The XRD pattern clearly corresponds to the cubic spinel structure of $MgAl_2O_4$ (JCPDS 21-1152), with sharp peaks and no impurity phases, indicating that the powder is well crystallised and phase-pure. The UV–Vis spectrum is consistent with this: significant UV absorption and almost no visible absorption are typical of a wide-band-gap, optically transparent oxide such as $MgAl_2O_4$.

The TEM images reveal that at the nanoscale the material is composed of rounded grains of around 100–300 nm that are highly crowded and partially fused together, while the patchy rings of the SAED pattern confirm that these grains are crystalline, which matches the XRD finding. Zooming out to the SEM images, the same material appears as uneven, angular, broken pieces a few to tens of micrometers wide, with surfaces coated in the same small, rounded particles seen in the TEM. The SEM and TEM images therefore fit together well, albeit at different length scales.

Finally, the EDX analysis shows that the powder is composed entirely of oxygen, magnesium and aluminium, with no impurities detected. The Mg:Al atomic ratio is about 1:1.4, which is Al-poor compared with the ideal 1:2 of stoichiometric $MgAl_2O_4$. A deviation of this size is common in EDX measurements because the technique probes only a small, localized area of the surface rather than the bulk average, and it can be influenced by particle shape and surface roughness. Nonetheless, the elements present and their approximate proportions confirm the identification of the material as $MgAl_2O_4$.

The photocatalytic tests add a caveat to this picture. The powder removed more than 96.5% of the 200 ppm dye at every dosage, but the light and dark results were close, so adsorption on the large, agglomerated particles accounts for most of the removal. The extra removal under light was about 2 percentage points at most. This agrees with the UV–Vis spectrum, which shows almost no visible absorption, since the LED source is mainly visible.

Overall, the XRD, UV–Vis, TEM, SEM and EDX results all point to the same conclusion: calcining the precursor at 800 °C successfully produces phase-pure, crystalline $MgAl_2O_4$ spinel, present as nanoscale grains that aggregate into larger, irregular, micrometer-sized clusters that remove azo dye mainly by adsorption, with a small light-driven contribution.

4. CONCLUSION

$MgAl_2O_4$ nanoparticles were successfully prepared by solution combustion of magnesium and aluminium nitrates with urea, followed by calcination at 800 °C. XRD, SAED, UV–Vis, TEM, SEM and EDX together show a phase-pure, crystalline cubic spinel made of nanoscale grains (about 100–300 nm) that aggregate into larger, irregular clusters. EDX found only O, Mg and Al, and the Al-poor Mg:Al ratio of about 1:1.4 most likely reflects the small area probed. Coralene Dark Red 2B (200 ppm) was removed by more than 96.5% at every dosage within 180 min, with a maximum of 99.8% under LED light and 99% in the dark. Light and dark removal were almost identical at low dosages, and the light advantage appeared only at some higher dosages and stayed at about 2 percentage points or less, so adsorption was the main removal route. The specific removal capacity fell steeply with dosage, from about 157 g g^{-1} to about 2.5 g g^{-1} in the light. $MgAl_2O_4$ made by this simple, low-cost combustion route is an effective material for removing azo dye from water, mainly through adsorption with a small photocatalytic contribution. Future work should test reusability, determine the band gap, check mineralization by COD or TOC measurements, and try a UV or solar source to see whether the light effect grows.

REFERENCES

1. Ahmad, A., Mohd-Setapar, S. H., Chuong, C. S., Khatoon, A., Wani, W. A., Kumar, R., & Rafatullah, M. (2015). Recent advances in new generation dye removal technologies: Novel search for approaches to reprocess wastewater. RSC Advances, 5(39), 30801–30818. https://doi.org/10.1039/C4RA16959J
2. Lellis, B., Fávaro-Polonio, C. Z., Pamphile, J. A., & Polonio, J. C. (2019). Effects of textile dyes on health and the environment and bioremediation potential of living organisms. Biotechnology Research and Innovation, 3(2), 275–290. https://doi.org/10.1016/j.biori.2019.09.001
3. Berradi, M., Hsissou, R., Khudhair, M., Assouag, M., Cherkaoui, O., El Bachiri, A., & El Harfi, A. (2019). Textile finishing dyes and their impact on aquatic environs. Heliyon, 5(11), Article e02711. https://doi.org/10.1016/j.heliyon.2019.e02711
4. Yaseen, D. A., & Scholz, M. (2019). Textile dye wastewater characteristics and constituents of synthetic effluents: A critical review. International Journal of Environmental Science and Technology, 16(2), 1193–1226.
5. Hoffmann, M. R., Martin, S. T., Choi, W., & Bahnemann, D. W. (1995). Environmental applications of semiconductor photocatalysis. Chemical Reviews, 95(1), 69–96. https://doi.org/10.1021/cr00033a004
6. Fujishima, A., & Honda, K. (1972). Electrochemical photolysis of water at a semiconductor electrode. Nature, 238(5358), 37–38. https://doi.org/10.1038/238037a0
7. Madhusudhana, N., Yogendra, K., & Mahadevan, K. M. (2014). Photocatalytic decolorization of textile effluent by using synthesized nano particles. Journal of Environmental Nanotechnology, 3(4), 41–53.
8. Santhosh, A. M., Yogendra, K., Mahadevan, K. M., Mallikarjuna, I. H., & Madhusudhana, N. (2018). Efficiency of photodegradation properties of nickel calciate nanoparticle synthesized by solution combustion method. International Journal of Scientific Research in Physics and Applied Sciences, 6(5), 48–56.
9. Sinhamahapatra, S., Das, P., Dana, K., & Tripathi, H. S. (2022). Magnesium aluminate spinel: Structure, properties, synthesis and applications. Transactions of the Indian Ceramic Society, 81(3), 97–120.
10. Ganesh, I. (2013). A review on magnesium aluminate ($MgAl_2O_4$) spinel: Synthesis, processing and applications. International Materials Reviews, 58(2), 63–112.
11. Parvarinezhad, S., Salehi, M., & Khademinia, S. (2019). Solid state synthesis of $MgAl_2O_4$ nanomaterials and solar light-induced photocatalytic removal of Malachite green. International Journal of Nano Dimension, 10(1), 89–104.
12. Shilpa, G., Yogendra, K., Mahadevan, K. M., Madhusudhana, N., & Santhosh, A. M. (2018). A comparative study over degradation of direct green 6 by using synthesized magnesium aluminate and magnesium zincate nanoparticles. IOSR Journal of Applied Chemistry, 11(5), 1–8.
13. Veena, S. R., Yogendra, K., Madhusudhana, N., & Latha, C. (2022). A preliminary investigation on photocatalytic degradation of Coralene Blue BGFS dye by using synthesized magnesium zinc aluminate nanoparticle in presence of UV light. Journal of Biological Innovations, 11(3), 689–701. https://doi.org/10.46344/JBINO.2022.v11i03.10
14. Qian, X., Li, B., Mu, H., Ren, J., Liu, Y., Hao, Y., & Li, F. (2017). Deep insight into the photocatalytic activity and electronic structure of amorphous earth-abundant $MgAl_2O_4$. Inorganic Chemistry Frontiers, 4(11), 1832–1840. https://doi.org/10.1039/C7QI00478H
15. Nassar, M. Y., Ahmed, I. S., & Samir, I. (2014). A novel synthetic route for magnesium aluminate ($MgAl_2O_4$) nanoparticles using sol–gel auto combustion method and their photocatalytic properties. Spectrochimica Acta Part A: Molecular and Biomolecular Spectroscopy, 131, 329–334. https://doi.org/10.1016/j.saa.2014.04.040
16. Serivalsatit, K., Teerasoradech, S., & Saelee, A. (2012). Synthesis of magnesium aluminate spinel nanoparticles by co-precipitation method: The influences of precipitants. Suranaree Journal of Science and Technology, 19(4), 265–270.
17. Patil, K. C., Aruna, S. T., & Mimani, T. (2002). Combustion synthesis: An update. Current Opinion in Solid State and Materials Science, 6(6), 507–512.
18. Aruna, S. T., & Mukasyan, A. S. (2008). Combustion synthesis and nanomaterials. Current Opinion in Solid State and Materials Science, 12(3–4), 44–50.
19. Varma, A., Mukasyan, A. S., Rogachev, A. S., & Manukyan, K. V. (2016). Solution combustion synthesis of nanoscale materials. Chemical Reviews, 116(23), 14493–14586. https://doi.org/10.1021/acs.chemrev.6b00279

20. Bhaduri, S., Bhaduri, S. B., & Prisbrey, K. A. (1999). Auto ignition synthesis of nanocrystalline $MgAl_2O_4$ and related nanocomposites. Journal of Materials Research, 14(9), 3571–3580.
21. [21] Ganesh, I., Johnson, R., Rao, G. V. N., Mahajan, Y. R., Madavendra, S. S., & Reddy, B. M. (2005). Microwave-assisted combustion synthesis of nanocrystalline $MgAl_2O_4$ spinel powder. Ceramics International, 31(1), 67–74.
22. [22] Carvalho, L. S., Melo, V. R. de M. e, Sobrinho, E. V., Ruiz, D., & Melo, D. M. de A. (2018). Effect of urea excess on the properties of the $MgAl_2O_4$ obtained by microwave-assisted combustion. Materials Research, 21(1), Article e20170189. https://doi.org/10.1590/1980-5373-MR-2017-0189
23. Rahaman, M. N. (2003). Ceramic processing and sintering (2nd ed.). Marcel Dekker.
24. Kalasapur, V. V., Aravinda, T., Kumar, B. V., Kugaji, M., & Madhusudhana, N. (2026). Green synthesis of indenone chalcones using recyclable Sr–Ca mixed oxide nanocatalyst with preliminary in vitro anticancer screening. Chemical Papers. https://doi.org/10.1007/s11696-026-05171-z
25. Cullity, B. D., & Stock, S. R. (2001). Elements of X-ray diffraction (3rd ed.). Prentice Hall.
26. Williams, D. B., & Carter, C. B. (2009). Transmission electron microscopy: A textbook for materials science (2nd ed.). Springer.
27. Goldstein, J. I., Newbury, D. E., Michael, J. R., Ritchie, N. W. M., Scott, J. H. J., & Joy, D. C. (2018). Scanning electron microscopy and X-ray microanalysis (4th ed.). Springer.
28. Jain, S. R., Adiga, K. C., & Pai Verneker, V. R. (1981). A new approach to thermochemical calculations of condensed fuel–oxidizer mixtures. Combustion and Flame, 40, 71–79.
29. International Centre for Diffraction Data. (n.d.). Powder diffraction file: Card No. 21-1152, $MgAl_2O_4$ (magnesium aluminum oxide, spinel) [Reference card]. https://www.icdd.com
30. Perkampus, H.-H. (1992). UV-VIS spectroscopy and its applications. Springer.
31. Fultz, B., & Howe, J. M. (2013). Transmission electron microscopy and diffractometry of materials (4th ed.). Springer.
32. Egerton, R. F. (2005). Physical principles of electron microscopy: An introduction to TEM, SEM, and AEM. Springer.
33. Newbury, D. E., & Ritchie, N. W. M. (2013). Is scanning electron microscopy/energy dispersive X-ray spectrometry (SEM/EDS) quantitative? Scanning, 35(3), 141–168. https://doi.org/10.1002/sca.21041
34. Li, F.-T., Zhao, Y., Liu, Y., Hao, Y.-J., Liu, R.-H., & Zhao, D.-S. (2011). Solution combustion synthesis and visible light-induced photocatalytic activity of mixed amorphous and crystalline $MgAl_2O_4$ nanopowders. Chemical Engineering Journal, 173(3), 750–759. https://doi.org/10.1016/j.cej.2011.08.043
35. Reimer, L. (1998). Scanning electron microscopy: Physics of image formation and microanalysis (2nd ed.). Springer.
36. Ahmed, S., Rasul, M. G., Martens, W. N., Brown, R., & Hashib, M. A. (2011). Influence of parameters on the heterogeneous photocatalytic degradation of pesticides and phenolic contaminants in wastewater: A short review. Journal of Environmental Management, 92(3), 311–330. https://doi.org/10.1016/j.jenvman.2010.08.028
37. Chong, M. N., Jin, B., Chow, C. W. K., & Saint, C. (2010). Recent developments in photocatalytic water treatment technology: A review. Water Research, 44(10), 2997–3027. https://doi.org/10.1016/j.watres.2010.02.039
38. Herrmann, J.-M. (1999). Heterogeneous photocatalysis: Fundamentals and applications to the removal of various types of aqueous pollutants. Catalysis Today, 53(1), 115–129. https://doi.org/10.1016/S0920-5861(99)00107-8
39. Konstantinou, I. K., & Albanis, T. A. (2004). TiO_2-assisted photocatalytic degradation of azo dyes in aqueous solution: Kinetic and mechanistic investigations: A review. Applied Catalysis B: Environmental, 49(1), 1–14. https://doi.org/10.1016/j.apcatb.2003.11.010